AD_____

Award Number: DAMD17-98-1-8157

TITLE: A Low-Cost, High Quality MRI Breast Scanner Using Prepolarization

PRINCIPAL INVESTIGATOR: Albert Macvoski, Ph.D.

CONTRACTING ORGANIZATION: Stanford University
Stanford, California 94350-3027

REPORT DATE: October 2001

TYPE OF REPORT: Final

PREPARED FOR: U.S. Army Medical Research and Materiel Command
Fort Detrick, Maryland 21702-5012

REPORT DOCUMENTATION PAGE

Form Approved
OMB No. 074-0188

1. AGENCY USE ONLY (Leave blank)	2. REPORT DATE	3. REPORT TYPE AND DATES COVERED
	October 2001	Final (01 Oct 98 - 30 Sep 01)

4. TITLE AND SUBTITLE
A Low-Cost, High Quality MRI Breast Scanner Using Prepolarization

5. FUNDING NUMBERS
DAMD17-98-1-8157

6. AUTHOR(S)
Albert Macovski, Ph.D.

7. PERFORMING ORGANIZATION NAME(S) AND ADDRESS(ES)
Stanford University
Stanford, California 94305-3027

E-Mail: Macovski@mrsrl.stanford.edu

8. PERFORMING ORGANIZATION REPORT NUMBER

9. SPONSORING / MONITORING AGENCY NAME(S) AND ADDRESS(ES)
U.S. Army Medical Research and Materiel Command
Fort Detrick, Maryland 21702-5012

10. SPONSORING / MONITORING AGENCY REPORT NUMBER

11. SUPPLEMENTARY NOTES
Report contains data on a floppy disk.

12a. DISTRIBUTION / AVAILABILITY STATEMENT
Approved for Public Release; Distribution Unlimited

12b. DISTRIBUTION CODE

13. ABSTRACT ***(Maximum 200 Words)***

Magnetic Resonance Imaging (MRI) has been shown to be more sensitive and equally specific when compared to x-ray mammography for detecting breast cancer. MRI is non-invasive, completely non-toxic, and requires no uncomfortable breast compression. But an x-ray mammogram costs about $100 whereas an MRI study costs about $1500. The exam cost is related to the scanner's manufacturing cost (about $400,000) and sale price (about $1 to $3 million). X-ray mammography units cost about one tenth of the cost of an MRI scanner.

Our objective is to tailor a new concept in MRI called Prepolarized MR (PMRI) for low-cost MR mammography. PMRI substitutes two inexpensive pulsed magnets for the expensive superconducting magnet. We believe that a high-quality MRI breast scanner using prepolarization could be manufactured for less than $45,000. This project could potentially make MRI as affordable as x-ray mammography.

We have made considerable progress this year in realizing a working PMRI scanner. Indeed, we recently obtained our first in vivo human wrist images with our 0.4T prototype scanner. While the image quality of our prototype scanner is not yet of clinical quality, the results are very promising considering the total cost of the magnets was less than $30,000.

14. SUBJECT TERMS
Breast cancer

15. NUMBER OF PAGES
27

16. PRICE CODE

17. SECURITY CLASSIFICATION OF REPORT	18. SECURITY CLASSIFICATION OF THIS PAGE	19. SECURITY CLASSIFICATION OF ABSTRACT	20. LIMITATION OF ABSTRACT
Unclassified	Unclassified	Unclassified	Unlimited

FOREWORD

Opinions, interpretations, conclusions and recommendations are those of the author and are not necessarily endorsed by the U.S. Army.

✓ Where copyrighted material is quoted, permission has been obtained to use such material.

✓ Where material from documents designated for limited distribution is quoted, permission has been obtained to use the material.

✓ Citations of commercial organizations and trade names in this report do not constitute an official Department of Army endorsement or approval of the products or services of these organizations.

Does NOT Apply In conducting research using animals, the investigator(s) adhered to the "Guide for the Care and Use of Laboratory Animals," prepared by the Committee on Care and use of Laboratory Animals of the Institute of Laboratory Resources, national Research Council (NIH Publication No. 86-23, Revised 1985).

✓ For the protection of human subjects, the investigator(s) adhered to policies of applicable Federal Law 45 CFR 46.

Does Not Apply In conducting research utilizing recombinant DNA technology, the investigator(s) adhered to current guidelines promulgated by the National Institutes of Health.

Does Not Apply In the conduct of research utilizing recombinant DNA, the investigator(s) adhered to the NIH Guidelines for Research Involving Recombinant DNA Molecules.

Does Not Apply In the conduct of research involving hazardous organisms, the investigator(s) adhered to the CDC-NIH Guide for Biosafety in Microbiological and Biomedical Laboratories.

Albert Macovski 10/31/2001

PI - Signature Date

4 Table of Contents

5 Introduction

The objective of this research is to develop a new concept in magnetic resonance imaging called Prepolarized MRI (PMRI) for low-cost MR mammography. Although MRI has been shown to be useful for the noninvasive diagnosis of breast cancer, x-ray mammography remains dominant because a typical MRI study costs more than ten times as much as an x-ray mammogram. We believe that a high-quality MRI breast scanner using our new concept of prepolarization could be manufactured for less than $50,000, which is about 10% of the manufacturing cost of a conventional MRI scanner.

Breast imaging presents several unique technical challenges for the PMRI concept. First, we must accommodate the patient's torso into the magnet configuration. Second, since breast tissue is relatively nonconductive we will need to use extremely sensitive receiver coils to obtain optimal image quality. Finally, we will need to develop PMRI pulse sequences that suppress fat and provide high quality 3D images.

We have made significant progress toward the goal of a prepolarized MRI scanner for human breast imaging. We made the first ever low-cost *in vivo* human prepolarized MRI image. The only previous Prepolarized *in vivo* image was performed on a relatively expensive Toshiba scanner. This breakthrough is very encouraging for the development of a prepolarized MRI breast scanner. Moreover, these promising results have produced significant funding from the NIH to build a head and knee PMRI scanner.

6 Body

This section gives the results of our preliminary Prepolarized MRI experiments, which were supported in part by NIH grant R21 CA79728. First we demonstrate that increas-

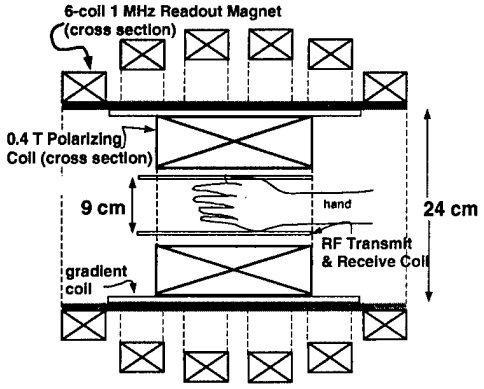

Figure 1: Sketch of our prototype 9-cm-bore Prepolarized MRI scanner used for imaging the human wrist *in vivo*. The strong (0.4 T at 100 A) polarizing magnet is coaxial with and inside the low-field (25 mT, or 1 MHz NMR frequency) readout magnet. The total cost of the magnets shown here was less than $20,000.

ing the polarizing field increases the SNR for both NMR free induction decay (FID) signals and MR images. We then show that PMRI has contrast similar to, and perhaps more flexible than, standard MRI. Then we demonstrate the typical quality of our human *in vivo* PMRI wrist images. Finally we detail the custom hardware components of the PMRI scanner.

Overview of the Stanford PMRI Scanner The diagram in Fig. 1 shows the Stanford Prepolarized MRI prototype wrist scanner. We built a 13-cm-bore, 0.4 T polarizing magnet [1], a 24-cm-bore 3-axis gradient coil set [2], and a transmit-receive litz wire RF coil. The overall system [3] (Appendix 9) is described in detail in the next section.

6.1 PMRI SNR Studies

There are two factors in Signal-to-Noise Ratio: signal and noise. In the following paragraphs we will demonstrate that: (1) the PMRI signal is linearly dependent on the strength of the polarizing field, and (2) the SNR in PMRI images does not increase with readout field strength beyond the frequency at which body noise dominance is attained. We will also emphasize the fact that the fundamental SNR field strength dependencies valid for traditional NMR and MRI are significantly different for PMRI. As discussed in the "Noise Experiments" section, of primary importance is the fact that above a certain frequency (at which body noise dominance is achieved), PMRI SNR is dependent solely on the polarizing field strength.

6.1.1 Signal Strength Experiments

FID Strength Experiments One would expect a linear increase in the NMR signal as a function of the polarizing magnetic field. To verify this experimentally, we collected a set of free induction decay (FID) curves using a pulse sequence with a variable amplitude polarizing field. The experiment was conducted using a small water phantom doped with $CuSO_4$ to achieve short relaxation times. The polarizing pulse was applied for a duration of 600 ms, several times longer than the phantom T_1 at the highest polarizing field, thereby guaranteeing nearly full sample polarization at the end of the polarizing pulse. The largest polarization pulse applied was 0.58 T. Immediately following the end of the polarizing pulse, a 90-degree RF pulse was applied and the signal was collected under the influence of the readout magnetic field alone. The strength of the readout magnet was set to 22 mT (1 MHz center frequency) during these experiments. For each polarizing field amplitude, the initial magnitude of the resulting FID was recorded.

The results of this experiment are shown in Fig. 2. The horizontal axis represents the total applied polarizing magnetic field, normalized to the strength of the readout field alone. The vertical axis represents the measured FID signal magnitude normalized to the FID signal obtained with no extra polarizing field ap-

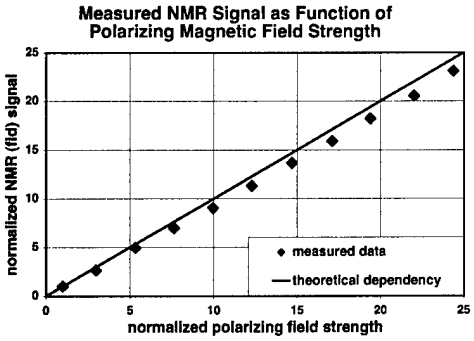

Figure 2: Experimental measurements of the free induction decay (FID) signal amplitude as a function of the applied polarizing field, for a $CuSO_4$ doped water sample. The axes are normalized to the field and FID signal obtained using the 1 MHz readout field alone. The slope closely matches the theoretical slope of 1.

plied (*i.e.* with only the readout magnet creating polarization). The data was fit to a linear curve, yielding an R^2 value of 0.9997. The slope of the fit is 0.94, demonstrating the realization of 94% of the theoretically expected linear increase in signal. This clearly demonstrates that the polarizing field can boost the NMR signal dramatically, in this experiment by a factor of more than 20.

Initial Imaging SNR Experiments Last year we collected the first images from our current prototype PMRI system. In order to demonstrate that image signal is also proportional to the polarizing field strength, we collected images of phantoms with and without applying a polarizing magnetic field. The images are shown in Fig. 3. The phantoms were two test tubes filled with water doped with copper sulfate. The two test tubes are approximately 1 cm in diameter and 3 cm deep. Imaging was performed with a two-dimensional Fourier transform (2DFT) sequence with gradient-recalled echoes. Both images were not slice selective. For both images, the effective echo time was 10.2 ms, the TR was 600 ms, and total imaging time was 51 seconds. The image on the right had a 0.5 T polarizing pulse on during the TR time. Both had a 1 MHz (22 mT) readout frequency. The image on the right using the 0.5 T polarizing field had a measured SNR 23 times greater than the SNR of the image on the left with a 22 mT static field, as expected from the linear increase in magnetization with field strength. This was a very encouraging milestone for our project because it demonstrates that we have an operational imaging system whose image quality is improved dramatically with the application of a polarizing field pulse.

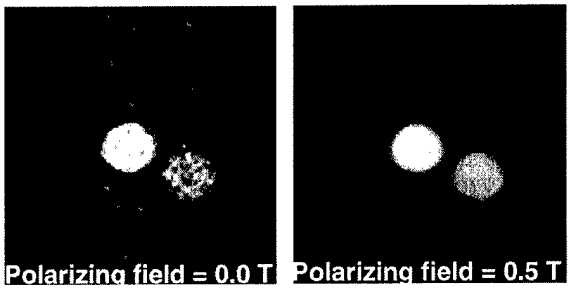

Figure 3: Experimental PMRI images demonstrating the SNR increase by applying a 0.5 T 600 ms polarizing pulse. The FOV for both images is 5 cm, and the matrix size is 64x64, for image resolution of 0.8 mm by 0.8 mm. The readout frequency for both images was 1 MHz. Total imaging time was 51 seconds for both images. Phantom was two test tubes filled with water doped to a T_1, T_2 = 50 ms and T_1, T_2 = 100 ms. The SNR was increased by 23 times by using the polarizing pulse.

6.1.2 Noise Experiments

In all forms of NMR, the dependence of SNR on the readout frequency is itself dependent on what source of noise is dominant. It is common to identify three main sources of noise or loss: resistance in the receive coil itself, magnetically coupled losses from the sample,

and electrically coupled losses from the sample [4, 5]. Each loss mechanism contributes a voltage noise power proportional to its effective resistance in the coil circuit. The electrically coupled losses from the sample can be avoided through careful RF coil design and possibly the use of a Faraday shield; therefore, we will only consider coil and magnetically coupled body losses in the following discussion. These two losses have different readout frequency dependencies. The most common situation for high field NMR is to have the coil noise dominating all noise sources (coil noise dominance). This results in the SNR of the system varying as the readout frequency to the 7/4 power. The most common situation for mid and high field MRI is to have the magnetically coupled losses from the sample dominating other noise sources (body noise dominance). This gives the well known result that the SNR of the system varys linearly with the readout frequency.

In PMRI, the equilibrium magnetization in the sample is independent of the readout field strength and depends linearly on the polarizing field strength. The same two regimes of noise-dominance mentioned above exist in PMRI, although their consequences are very different. For coil dominated noise, the SNR for PMRI varies with the readout frequency to the 3/4 power and linearly with the strength of the polarizing field. For sample dominated noise, the SNR for PMRI is *independent of the readout frequency* and linearly dependent on the polarizing field strength. This dependency is of fundamental importance to PMRI. Operating at a readout frequency below the coil-noise to body-noise dominance transition is suboptimal from an SNR standpoint. Operating at a readout frequency above the transition means more power than necessary is being dissipated in the readout magnet. The situation is even more favourable when the frequency dependence of tissue conductivity is considered. Tissue conductivity below 4 MHz is only about half that above 50 MHz [6, 7]. This basically means that tissue is fundamentally "noisier" at higher readout frequencies. Taking this into account, our PMRI SNR should be identical to an *ideal* mid-field system even if the receiver components contribute half the noise. For all of these reasons, it is extremely important to experimentally determine the frequency at which an RF coil makes the transition from coil noise dominance to body noise dominance.

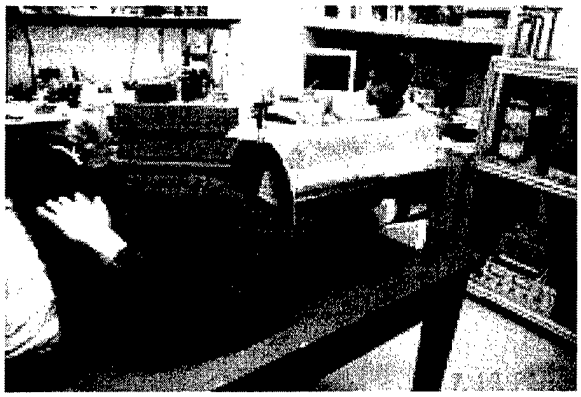

Figure 4: Experimental setup to measure coil Q with a network analyzer. Patient loading dominated other losses above 5 MHz, indicating that low-field readout will cause no significant loss of SNR.

The quality, Q, of an RF coil is a measure of the total magnetic energy versus losses acting in the resonant circuit. If two coils have the same geometry, the lower Q coil will have higher losses and poorer signal sensitivity. The comparison of measured coil Q values with and without a sample within the coil gives a measure of the relative noise contributions from the coil and the body. If we define a "loading factor": $lf = 1 - Ql/Qu$, then a lf value of 0.5 or greater indicates that over half of the total noise power in the circuit is due to the sample loading. We will define this situation as body noise dominance.

We measured coil Q as a function of frequency (between 1-10MHz) for a human head

size RF saddle coil (inner diameter: 235mm, shield diameter: 340mm) with and without the presence of a human head loading the coil (Fig. 4) and calculated the corresponding loading factor described above. The unloaded coil Q reached an optimum value of approximately 650 at a frequency of 8MHz before declining due to radiation losses and wavelength effects (Fig. 5). We observed very small shifts in the coil tuned frequency when the subject's head was placed within the coil, indicating that electrically coupled tissue losses were not significant. Our results indicate that patient loading exceeds all other losses for frequencies above 5 MHz. This is a milestone result, indicating that our low-field reception will cause no significant SNR degradation.

6.2 Contrast Studies

Our preliminary contrast studies were focused on three primary questions. The first question was to determine how much of the magnetization is lost during the polarizing magnet rampdown. The rate of the rampdown cannot exceed the FDA limit of 20 T/s, so it was important to determine if we would lose a great deal of the magnetization before imaging could occur. The second question was whether PMRI can obtain conventional T_1 and T_2 contrast. The third question was whether Prepolarized MRI can measure T_1 dispersion, the variation in T_1 with field strength.

MRI's excellent soft tissue contrast is based on the differences between T_1 and T_2 relaxation times in diseased and normal states. Prepolarized MRI image contrast is slightly more complicated than normal MRI. The three important relaxation intervals are illustrated in Fig. 6.

First, the buildup of longitudinal magnetization is governed by the time-varying T_1 during the polarizing pulse. Although the relaxation process is time-varying due to T_1 dispersion, this process obtains something very close to high-field T_1 contrast. Hence, short

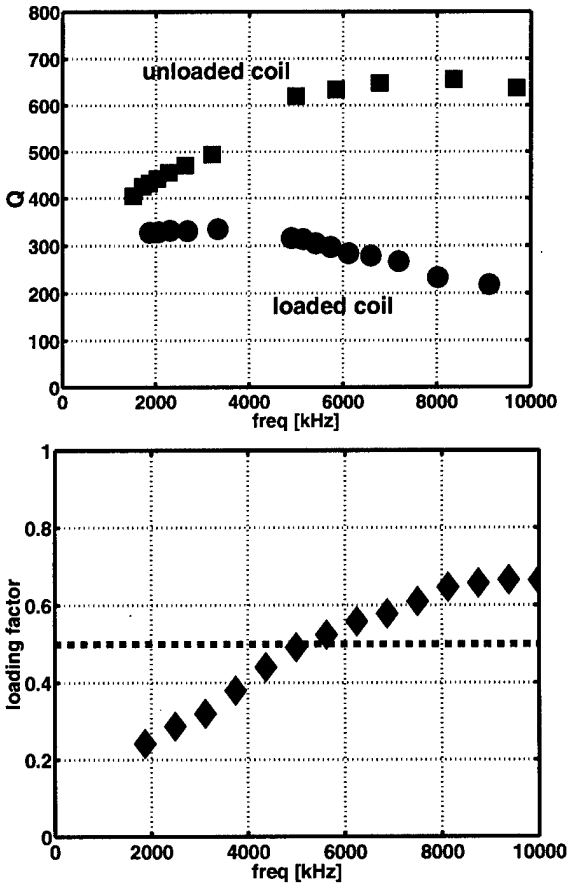

Figure 5: Loaded and unloaded coil Q measurement results for a shielded head saddle coil (top), and corresponding loading factor (lf = 1 - Ql/Qu) calculations (bottom). Our Q measurements demonstrate body noise dominance for realistic, shielded head coils at frequencies above 5 MHz. The load factor shows that 50% to 70% of the total losses arise from the human head above 5 MHz.

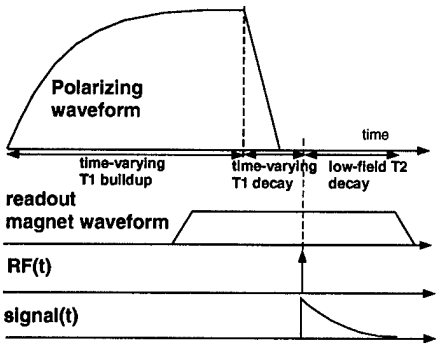

Figure 6: Timing diagram illustrating the different relaxation processes and timing intervals for Prepolarized MRI.

Figure 7: PMRI gradient echo image of a piece of bacon, demonstrating conventional fat-tissue image contrast. The matrix size was 64x64, 5 cm FOV, 780x780 μm in-plane resolution, 23.6 ms effective echo time, no averages, and a total imaging time of 30.1 s. No slice select was applied because the bacon slice was only about 4 mm thick. The polarizing pulse was applied at an amplitude of 0.55 T for 200 ms, allowing for T_1 image weighting. The fat is clearly brighter than the muscle.

polarizing pulses produce relatively brighter signal from short-T_1 species. As the polarizing pulse ramps down, and before the low-field RF excitation, longitudinal magnetization decays with a time-varying T_1 toward a time-varying equilibrium. After the RF pulse, transverse magnetization decays with low-field T_2, which is similar to high-field T_2.

Loss of Magnetization during Polarizing Field Rampdown The image quality of Prepolarized MRI is critically related to the amount of magnetization decay during the polarizing magnet rampdown. Using the instantaneous relaxation form of the Bloch equation, we found in a simulation study and experiments on the Valhalla hospital field-cycling spectrometer [8] that less than 20% of the magnetization was lost if we ramp the polarizing magnet down faster than 100 ms. This is within the FDA dB/dt limits of 20 T/s provided the maximum field is less than 2.0 T.

Conventional T_1 Contrast By reducing the duration of the polarizing interval, it is possible to create a fairly conventional T_1-weighted image. This is demonstrated in Fig. 7. In the next section we show T_2-weighted images obtained with spin echoes.

T_1 Dispersion Measurements It is well known that the T_1 of biological tissues generally increases with polarizing field strength, whereas T_2 is generally invariant to magnetic field strength. There are a few exceptions, *e.g.* deoxygenated blood T_2 is longer at low field. These variations in relaxation have been measured using field-cycling spectrometers, which are the non-imaging precursors to Prepolarized MRI. The relaxometry studies include blood [9, 10, 11, 12], gray and white matter [13], liver and skeletal muscle [14], and Bottomley's compendium [15].

We recently made measurements of the T_1 variation with field strength for canola oil and chicken muscle with our PMRI scanner. We varied both the duration and the amplitude of the polarizing pulse and recorded the peak strength of the FID signal. We fit the data to an exponential increase in magnetization. We

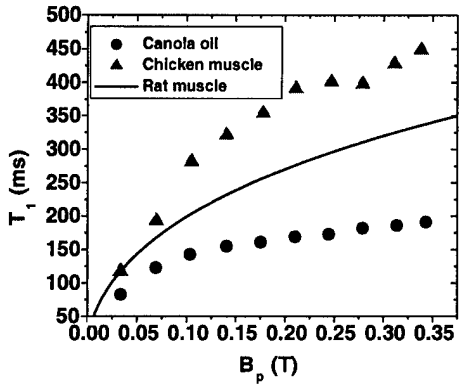

Figure 8: The variation in T_1 with field strength for canola oil and chicken muscle measured on our wrist-sized Prepolarized MRI scanner. The solid line is a curve fit to rat muscle T_1 dispersion data from [11].

then extracted the T_1's at ten different field strengths. The results are shown in Fig. 8. The chicken muscle dispersion data is also compared in this plot with a data fit for rat muscle tissue from [11]. The chicken muscle and the rat muscle have similar functional dependence, as one might expect.

6.3 In Vivo Human Wrist Images

Some representative *in vivo* human images are shown in Figs. 9, 10 and 11. These images were collected using a typical MR pulse sequence (save for the use of switched polarizing and readout magnetic fields), with reasonable acquisition times. The experience was described as comfortable by the volunteer subjects. The images shown are of the human wrist. Note that with a readout frequency of 1.1 MHz, we were not able to achieve body noise dominance with a hand-sized object. In §D, we plan to improve the wrist image SNR by using our second-generation readout magnet, which can operate at up to 8 MHz readout frequency.

Figure 9: Axial PMRI *in vivo* image of a normal human hand. A spin echo sequence was used with a 128x128 image matrix, 12 cm FOV, 1 cm slice, 34 ms echo time, 4 NEX and total scan time of 4 minutes. A polarizing pulse of 0.30 T was applied for 300 ms for T_1 contrast. The small bones and tendons of the hand are visible.

6.4 PMRI Instrumentation

We have built a wrist PMRI system, and we now have convincing evidence that Prepolarized MRI offers a significant reduction in capital cost relative to a conventional MRI scanner. Table 1 summarizes the capital costs of the unique elements of our prototype system. For donated components, we have listed the cost to construct a substitute system.

We also purchased a commercial Tecmag Apollo Low-Field imaging console. This console cost more ($48,000) than the entire cost of the prototype. However, we are confident that a console can be built at lower cost because our earlier experience with building digital and RF transceiver hardware indicated that a basic PMRI console can be constructed for less than $2,000 [16, 17]. Also, the gradient amplifiers are much less expensive than those used for conventional whole-body MRI. Because the gradient radius is approximately

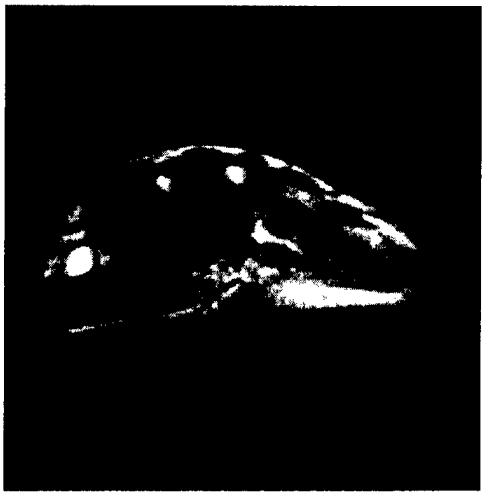

Figure 10: Axial PMRI *in vivo* image of a normal human hand. A spin echo sequence was used with a 128x128 image matrix, 12 cm FOV, 1 cm slice, 34 ms echo time, 2 NEX and total scan time of 3 minutes. A polarizing pulse of 0.35 T was applied for 300 ms for T_1 contrast. The small bones and tendons of the hand are visible.

Figure 11: Coronal PMRI *in vivo* image of a normal human wrist. A spin echo sequence was used with a 128x128 image matrix, 12 cm FOV, 1 cm slice, 34 ms echo time, 2 NEX and total scan time of 3 minutes. A polarizing pulse of 0.35 T was applied for 200 ms for T_1 contrast. The small bones of the wrist are visible.

halved, the same gradient strengths are possible with 30 times less power. There also could be significant savings on the RF screening of a PMRI scanner. Other low-field manufacturers (e.g., Esaote) have opted for conductive strips to shield the patient's knee rather than using a complete screen room.

Below we detail the requirements, preferred design, and results for each of our subsystems.

6.4.1 RF System

Since Prepolarized MRI uses a low-field readout magnet, signal detection is significantly more challenging than high frequency detection. PMRI requires a high Q receiver coil integrated with a matching network, and a preamplifier optimized for the largest possible SNR and bandwidth. To minimize sensitivity loss from the polarizing coil, an RF shield is also required. The transmitter coil must have a broad bandwidth to minimize distortion of selective RF excitation pulses. For our wrist prototype, we developed a dual mode transmit-receive coil that could achieve these requirements.

High Q Shielded Coils For our wrist prototype, we constructed a 9 cm diameter 4-turn litz saddle receiver coil which had an unloaded Q of 350 at 1.14 MHz. The litz wire (1725 separately insulated 48 AWG strands) effectively cheats the skin effect and requires less space than copper pipe of similar noise performance. The presence of the polarizing coil degraded the Q to 60 without additional RF shielding. After adding a 13 cm slotted copper sheet shield around the 9 cm wrist coil, the unloaded Q exceeded 250 in the polarizing magnet. The shield slots, located where the wrist coil RF image currents are zero, reduce gradient and polarizing coil eddy currents. The coil and shield are shown

Subsystem	wrist-scanner
Polarizing Magnet	$500
Polarizing Supply	$750
Readout Magnet	$17,000
Readout Supply	$5,000
Gradient Coils	$500
Gradient Amps	$4,500
RF Coils	$100
RF Amplifier	$1500
Total	$29,850

Table 1: Estimates of capital costs itemized for each of our two prototype scanners.

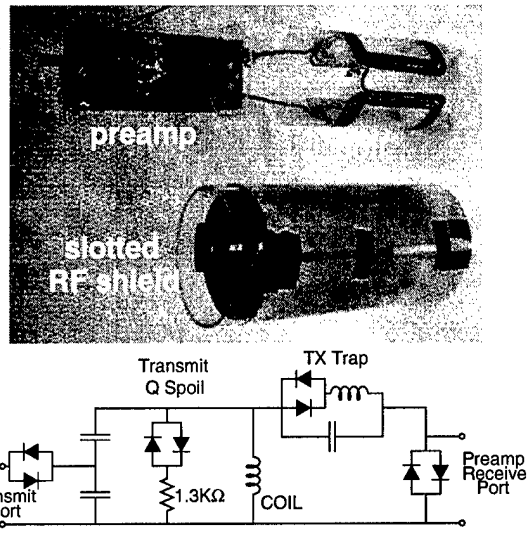

Figure 12: The dual transmit-receive wrist coil is a 4-turn saddle design with a 13 cm diameter slotted shield. The preamplifier is mounted directly on the matching circuit board for best SNR performance. The wrist imaging system transmit-receive coil circuit acts as a low Q (17) coil during transmit and a high Q (250) coil during receive.

in Fig. 12.

For feasibility tests, we also constructed larger 34 cm shields and 24 cm diameter saddle coils for testing coil loading factors. From this data, we determined that over 50% coil loading was achievable at 5 MHz for head imaging. In §D, we discuss new more efficient coil topologies for reducing the readout frequency threshold for body noise dominance.

Transmitter Q-spoiling A low field transmitter coil must have a coil bandwidth exceeding the RF excitation pulse bandwidth. We achieved this by a combination of cross-diode circuits that switch in under high power excitation. The coil circuits switched in a parallel resistive load to lower the coil Q, and an LC trap protected the preamplifier without loading the coil (Fig. 12). The capacitors are adjusted to give 50 Ω input impedance under high power conditions. When RF power is off, the diodes switch off, leaving the receive coil in a high Q, high SNR state.

Preamplifiers For maximum receiver bandwidth, an ultralow-noise preamplifier is crucial. Our first NMR experiments used a variation of a design by Fenzi [18] that employed a feedback resistor to synthesize a low "noiseless" input resistance. This technique flattens the signal (not the SNR) frequency response—a technique typically called feedback damping. The preamplifier was matched to the receive coil at a location that achieves the best overall combination of SNR and bandwidth [19].

Figure 13 shows the wrist coil tuning bandwidth in its transmit, receive, and unloaded modes of operation. We achieve broadened transmit and receive bandwidth suitable for PMRI.

6.4.2 Readout Magnet and Power Supply

Our first readout magnet was designed to create a 50-ppm homogeneous field over the 20-cm DSV (diameter spherical volume). In a compromise between higher readout magnet power and achieving body noise dominance, we chose to operate at a readout frequency

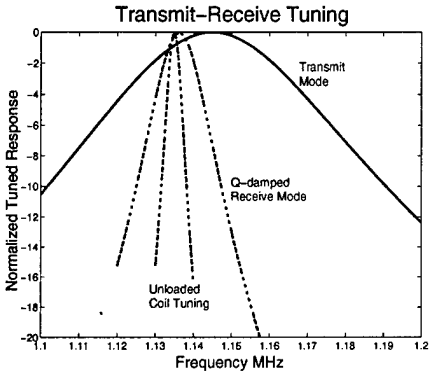

Figure 13: Wrist coil transmit-receive response. In transmit mode (solid), the coil Q is spoiled during high power pulses to minimize distortion of selective pulse shapes. In receive mode, the preamp damps the Q from its unloaded high Q state. The received signal is equalized without adding extra noise.

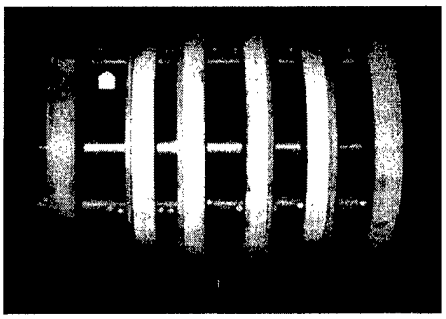

Figure 14: Photo of our $17,000 homebuilt 24-cm-bore, 23 mT, 2 kW homogeneous magnet for PMRI of extremities. After mechanical shimming, we measured 40 ppm homogeneity on axis.

of 1 MHz, or 22 mT field strength. The readout field must be temporally and spatially stable; thermal expansion of the magnet causes a significant downward drift in the resonant frequency.

Our first resistive homogeneous magnet was a variant of the classic 6-coil design [20, 21], with a 24-cm diameter free bore and 20-cm spherical homogeneous volume. Figure 14 shows a photograph of the magnet. The design and construction methods were described in [22] (Appendix 3), which was selected as a finalist for the ISMRM Rabi Award. Total cost for this magnet was $17,000, mostly due to machining costs. At 1 MHz the 110-kg magnet required a current of 13 A, dissipating approximately 2 kW (about two hair dryers). This magnet was used for all of the Prepolarized MRI data shown in this proposal.

We recently constructed a second generation magnet for knee imaging. Here, we designed a 31-cm-bore, 3 MHz readout magnet with a homogeneous cylindrical volume of axial length 12 cm and diameter 16 cm using the minimum power method in [23] (Appendix 8). To improve thermal stability, we added an effective water cooling system called edge-cooling [24, 25]. Even though this water-cooled magnet operates at three times the field of our previous generation magnet, it only dissipates 3.3 kW and the total construction price was only $6,720, or 40% of our wrist readout magnet. This new design demonstrates improvement in our magnet building skills. Figure 15 shows a photograph of the magnet, which was funded by our TRDRP grant. We found the water cooling to be effective, limiting the temperature rise to $35°C$ at the operating field strength.

The only major design effort remaining is to shim this magnet to better than 10 ppm over a knee-shaped homogeneous volume. In §D we describe a shim set for head imaging that ought to correct for most magnet machining errors.

Readout Magnet Supply The readout magnet current supply must meet stringent stability requirements. The field must be stable to within 10 ppm. The polarizing coil and the readout coil are highly coupled inductors, so transient waveforms in the polarizing magnet couple to the readout magnet. The read-

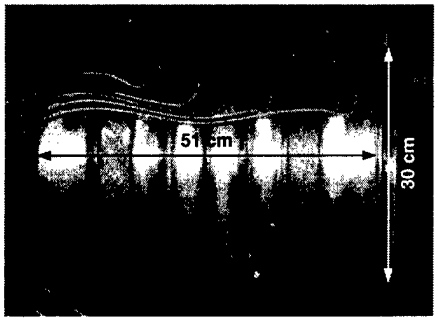

Figure 15: Photograph of our 31-cm-bore 3-MHz (70-mT) homogeneous knee readout magnet which was recently constructed for less than $7,000.

out magnet power supply must recover its 10 ppm field stability level in just a few milliseconds after the transient caused by the polarizing coil rampdown.

We recently constructed a readout supply that meets these stringent stability and transient recovery requirements [26]. It is also a pulsed power supply, active only during the 20% duty cycle of data acquisition. Compared to our prior DC stabilization system [27], magnet heating is reduced by a factor of five. This means we can pulse to over double the previous readout frequency for improved SNR and imaging speed.

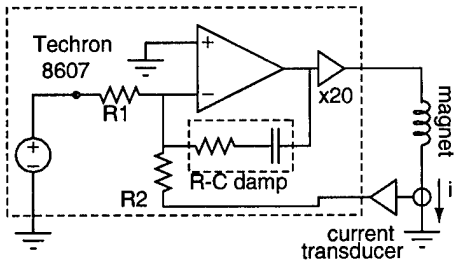

Figure 16: Readout supply using Techron amplifiers, which act like power op-amps. Current is sensed by a precision current transducer, and the RC damp circuit speeds up transient decay. This circuit can pulse our readout magnet to .18 T.

We converted a pair of Techron 8607 MRI gradient amplifiers into a pulsed readout current source capable of delivering up to 100 A with excellent stability. We can pulse the field on or off in about 15 ms, and the readout current is stabilized in just a few milliseconds after the polarizing rampdown.

The Techron amplifier appears complex, but we have shown that the simple electrical model shown in Fig. 16 is adequate to accurately predict its stability and transient performance.

The readout magnet is considerably different from a gradient coil, the usual load for the gradient amplifier. To convert the amplifier for this new load we modified the control circuit of the master gradient amplifier to sense magnet current with a Danfysik Ultrastab current transducer. This is more sensitive and more robust than resistive current feedback. We also carefully tuned the series resistor-capacitor network in the feedback compensation (labeled RC damp in Fig. 16) to provide the shortest possible recovery time to transients.

Minimizing Transients During the polarizing coil rampdown, a voltage is induced in the readout coil that can disturb the readout magnet current. Readout magnet field disturbances must decay below ppm levels within 5 ms of the end of the polarizing coil rampdown interval to allow for data acquisition in a homogeneous field. The magnet load has both inductance, L, and stray capacitance, C_0. Hence, any transients inevitably lead to ringing. This is an extremely significant problem, as the duration of this ringing transient is typically several hundred milliseconds, which would render PMRI impractical.

We recently discovered that one can significantly reduce the duration of this transient by choosing the amplifier feedback parameters to provide a *critically damped* response to transients [28]. Specifically, the feedback

must set the output capacitance to be 8 C_0 in series with an output resistance of 0.65 $\sqrt{L/C_0}$ [26]. For our 11Ω, 0.34 H magnet, a transient decay time of 226 μs is possible when the RC compensation components are adjusted to give the critical damping condition. Allowing for 14 time constants to guarantee all disturbances fall below ppm levels, we can record FIDs just 5 ms after the rampdown of the polarizing magnet. Before we used critical damping, we could not acquire NMR data within 100 ms of the polarizing rampdown. This wait severely attenuated the NMR signal.

Figure 17 shows experimental proof of the critical damping method. The polarizing magnet ramps down from 50 A (a), inducing a voltage exceeding 50 volts in the readout magnet (b). With critical damping the recovery time is under 5 ms (c), while the transient without critical damping response is disastrous (d).

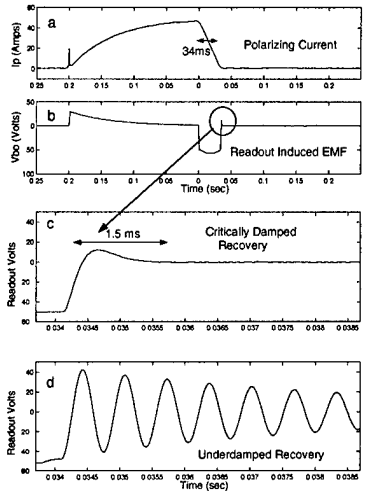

Figure 17: Experimental proof that critical damping minimizes the transient in the readout magnet. The polarizing current rampdown induces voltage (EMF) in the readout magnet and creates induced currents. A close-in oscilloscope trace at the end of rampdown shows that we can reduce these transients below 5 ms using our critical damping method. Otherwise, transients could remain for over 100 ms, which would be disastrous for Prepolarized MRI.

Tracking B_0 Field Drift Another major consideration was the combined stability of our readout magnet and pulsed supply with prolonged operation. As the magnet heats, thermal expansion progressively lowers the magnet field by up to 1 part per thousand. Second, the voltage references of our Techron 8607 amplifiers, which determine the readout supply current stability, were not designed for the level of precision required of PMRI. These phenomena cause short term phase shifts and a slow drift in the center frequency of FIDs in Fig. 18.

To minimize field drift artifacts, two measures were necessary. First, we appended an FID acquisition, called a frequency navigator, after each k-space scan. When Fourier transformed, the FID provided the instantaneous center frequency for that line of k-space. Figure 18 shows that in a typical scan, we had almost a 400 Hz drift. The field drift data was used to remove phase errors in the image reconstruction algorithm. The second improvement was the implementation of spin echo acquisition. The spin echo, to first order, cancelled drift on short time scales of 10 to 30 ms. Figure 19 demonstrates that spin echo images with field tracking FIDs (right) have almost no artifact in comparison to simple gradient echo images (left). These improvements significantly improved the robustness to field instability in our pulsed readout system.

In summary, we now have a reliable pulsed power supply that meets the Prepolarized MRI specifications. In addition, we have developed several methods that reliably suppress readout field transients and field drift.

6.4.3 Polarizing Magnet and Power Supply

The purpose of the polarizing magnet is to provide as strong a field as possible given

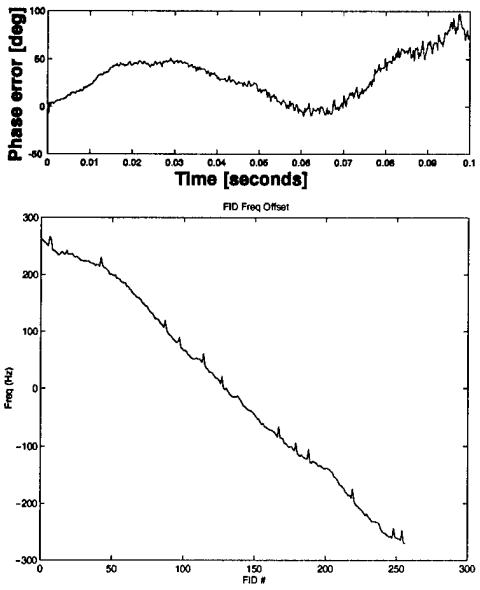

Figure 18: Top: The short term phase error superimposed on an FID signal is correctable with spin echo acquisitions. Bottom: Long term Larmor frequency drift vs acquisition. Magnet heating causes up to a 400 Hz drift but is measured and corrected with frequency navigators.

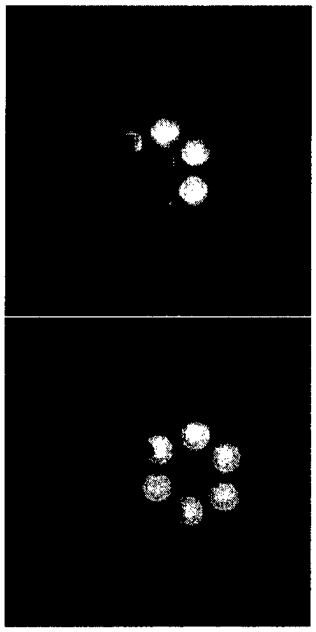

Figure 19: Severe ghosting occurs in the phase encode direction if the readout field is unstable as shown in the gradient echo image (left). By adding FID field tracking and spin echoes, both long term and short term drift errors are minimized (right).

power constraints. Fortunately, the spatial homogeneity requirement is quite relaxed. This is because differences in polarizing field strength cause only a corresponding variation in the local magnetization produced in the object, which results solely in a shading of the image. Hence, we can use a simple solenoid to generate the field.

To date, we have designed and constructed three polarizing magnets. In general, the inner bore is fixed by the size of the object to be imaged, and the outer bore and length are the two design variables. Our first design was a minimum-power geometry [24] solenoid, in which the outer bore is three times the inner bore and the length is twice the inner bore. These magnets tend to be fairly heavy and somewhat costly. Three years ago we developed a "minimum-cost" method for designing

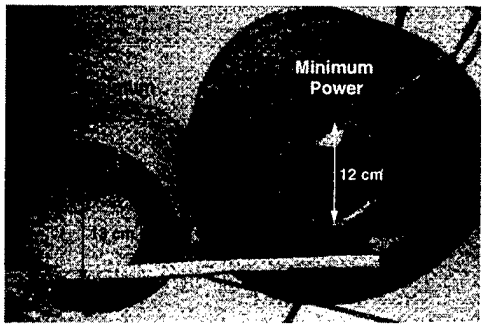

Figure 20: Photograph showing a minimum cost and a minimum power magnet. At 100 A, the minimum cost magnet acheives a 0.4 T field, dissipating 10 kW.

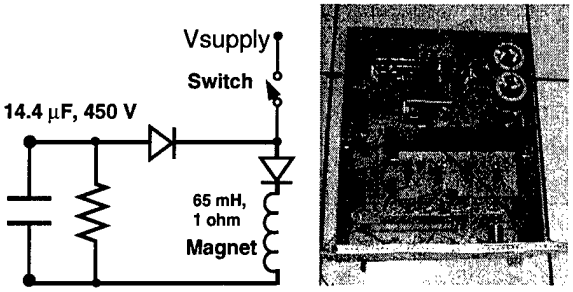

Figure 21: Our pulsing circuit diagram (left) and a photo of the circuit (right).

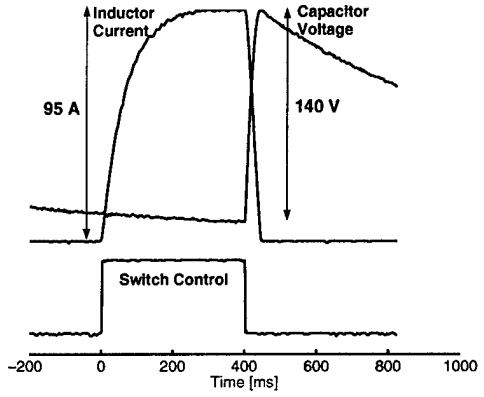

Figure 22: 100 A polarizing pulse (0.4 T) measured with an inductive current probe. Capacitor voltage also rises by 140 V as the stored energy is transferred in 65 ms.

solenoids [1]. Here we trade efficiency for dramatically reduced conductor mass. Figure 20 compares the results of the two design methods for wrist-sized polarizing magnets.

Our minimum-cost, wrist-sized polarizing magnet has a 13-cm bore. The outer diameter is 22 cm, and length is 21 cm. At 100 A, it creates a 0.4 T field strength, dissipating 10 kW. It has a mass of 42 kg, inductance of 65 mH, and resistance of 1 ohm. This magnet cost only $500.

Polarizing Magnet Pulsing Circuit The polarizing magnet supply requires both high power and fast switching electronics. Our wrist-sized coil dissipates 10 kW when operating at 0.4 T. Fortunately, we can tolerate poor current regulation, since the magnetization response time is limited by T_1 to hundreds of milliseconds. The most challenging specification is the current rampdown, which must be under 100 ms to limit unwanted magnetization decay during the rampdown [8]. A field holding several kilojoules of stored energy must be completely quenched (to less than a few microtesla) before RF excitation and signal acquisition. Otherwise, the dramatic inhomogeneity of the polarizing field will cause complete MRI signal dephasing.

To satisfy these constraints, we use a power switching circuit which efficiently transfers the coil energy to a capacitor with minimum dissipation in the semiconductor switch. We built a 100 A magnet pulsing circuit [29], shown in Fig. 21.

Figure 22 shows a 97 A polarizing coil pulse (0.4 T) and the capacitor voltage. This circuit cost only $750, most of which was due to the capacitors. This circuit is scalable, extremely robust, and inexpensive.

6.4.4 Gradient Design

Like conventional MRI systems, PMRI requires a three-axis gradient coil system. Gradient coil design and synthesis is an area of par-

Figure 23: Human head image collected using a three-axis gradient coil built by a member of our group, demonstrating our ability to design, fabricate, and use head-specific gradient coils.

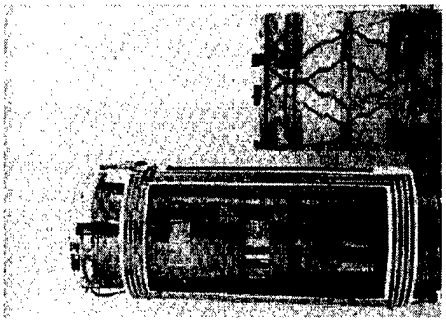

Figure 24: Photograph comparing the length of our minimum power gradient (top) with the classic Golay coil. The Golay set also incorporates transmit and receive coils.

ticular expertise in our group. We have designed, built, and tested different gradient coil sets for human head and neck imaging [?](Appendix 6), human breast imaging [?], and mouse imaging [?](Appendix 7). The gradient requirements for PMRI are in fact relatively easy to meet as compared to conventional MRI systems, and our first gradient system for PMRI was a simple Golay plus Helmholtz-pair gradient set using inexpensive copper tape layered over an acryllic tube.

Most relevent for this proposal, Blaine Chronik, a post-doc in our group, designed, built, and tested a head and neck gradient during his doctoral thesis under Dr. Brian Rutt [?]. A typical image of a human head collected with this coil is shown in Fig. 23. This coil was operated at field strengths from 0.5 T to 4.0 T and clearly demonstrates our capabilities in advanced gradient coil design and fabrication.

In §D we will show that for a dedicated head scanner there is a strong motivation to design the system with a narrower section for the head, and a wider section to admit the shoulders. Ideally the gradients should also fit this variable radius geometry. Most existing fast gradient design algorithms are restricted to conductors lying on a cylinder or a sphere [30, 31, 32]. Hence, we need a more flexible gradient design method. Numerical optimization has been developed for gradients mounted on arbitrary surfaces, but these require excessive computation time [33, 34, 35, 36, 37].

We recently generalized our minimum power homogeneous magnet algorithm to design gradient coils. We discovered that this design problem can be solved very efficiently with linear programming [2]. Our algorithm has several advantages over existing programs: no approximation is needed to implement the gradient after the design phase, the computation requires less than a minute, the coils typically have less than four loops, the power is minimized, and one can constrain the conductors to an arbitrary surface.

We recently built a constrained length gradient coil for our wrist scanner using this algorithm. The photo in Fig. 24 shows our constrained length gradient is about half as long as the Golay gradient, despite having a larger homogeneous gradient volume. This algorithm will help us to design a dedicated neuro gradient set.

6.5 Summary

The preliminary studies described above served to test the three fundamental assumptions of Prepolarized MRI. First, we presented data demonstrating that the expected linear increase in NMR signal with polarizing field is indeed observed. We verified this fact in imaging tests where the image SNR improved dramatically with the application of a 0.5 T polarizing field pulse. Second, normal tissue contrast was shown to be attainable with PMRI. T_1 dispersion measurements were carried out and indicated that strong muscle-fat contrast is expected over a full range of polarizing field strengths; furthermore, additional contrast, based on the different dispersion curves of these two typical tissue components, is possible. Fat-muscle contrast was also demonstrated in imaging tests of a bacon sample. Finally, we described in detail a complete functional PMRI scanner that was built by our group at Stanford. The total capital cost for this system was estimated to be $30,000. This supports the final and perhaps most important assumption underlying our PMRI project- that the system can be built at an extremely low cost. These positive preliminary results are the motivation for the proposed development of a human head PMRI scanner, outlined in the following section.

7 Conclusions

We are very encouraged by our recent progress making our first human *in vivo* wrist images on an ultra-low-cost MRI scanner. This has been an extremely challenging engineering development. Our initial images are very promising, but certainly not yet of clinical quality. Due to the promising preliminary data obtained under Army BCRP support, we have recently received NIH support to carry this research to larger body parts, including the knee and the head. We hope to develop a new ultra-low-cost form of high-quality MRI. Since cost is one of the key obstacles for replacing more invasive x-ray mammography, our ongoing research could have a major impact on the diagnosis and treatment of breast cancer.

References

[1] S. Conolly, G. Scott, and A. Macovski, Minimum-cost solenoid design for prepolarized MRI, *in* "Proceedings of the ISMRM", p. 255, March 1998.

[2] H. Xu, S. Conolly, G. Scott, and A. Macovski, Gradient design with arbitrary geometrical constraints by linear programming, *in* "Proceedings of the ISMRM", p. 747, April 1999.

[3] G. Scott, B. Chronik, N. Matter, H. Xu, P. Morgan, L. Wong, A. Macovski, and S. Conolly, A prepolarized MRI scanner, *in* "Abstracts of the Int. Soc. Magnetic Resonance,9th Annual Meeting", p. 610, Glasgow, April 2001. Intl. Soc. of Magnetic Resonance.

[4] D. Hoult and P. Lauterbur, The sensitivity of the zeugmatographic experiment involving human samples, *J. Magn. Reson.*, **34**, 425-433, (1979).

[5] D. Gadian and F. Robinson, Radiofrequency losses in NMR experiments on electrically conducting samples, *J. Magn. Reson.*, **34**, 449-455, (1979).

[6] K. Foster and H. Schwan, Dielectric properties of tissues and biological materials: A critical review, *Crit. Rev. Biomed. Eng.*, **17**, 25-104, (1989).

[7] R. Stoy, K. Foster, and H. Schwan, Dielectric properties of mammalian tissues from 0.1 to 100 MHz: a summary of recent data, *Phys. Med. Biol.*, **27**, 501-513, (1982).

[8] S. Conolly, R. Brown, and A. Macovski, SNR and dB/dt tradeoffs for prepolarized MRI, *in* "Proceedings of the Society of Magnetic Resonance", August 1995.

[9] T. Lindstrom and S. Koenig, Mangetic-field-dependent water proton spin-lattice relaxation rates of hemoglobin solutions and whole blood, *J. Magn. Reson.*, **15**, 344-353, (1974).

[10] R. Brooks and G. D. Chiro, Magnetic resonance imaging of stationary blood: A review, *Med. Phys.*, **8**, 903-913, (1987).

[11] R. G. Bryant, K. Marill, C. Blackmore, and C. Francis, Magnetic relaxation in blood and blood clots, *Magn. Reson. Med.*, **13**, 133-144, (1990).

[12] J. Gomori, R. Grossman, C. Yu-Ip, and T. Asakura, NMR relaxation times of blood: Dependence on field strength, oxidation state, and cell integrity, *Journal of Computer Assisted Tomography*, **11**(4), 684-690, (1987).

[13] H. Fischer, P. Rinck, Y. Haverbeke, and R. Muller, Nuclear relaxation of human brain gray and white matter: Analysis of field dependence and implications for MRI, *Magn. Reson. Med.*, **16**, 317-334, (1990).

[14] O. Henriksen, J. D. Certaines, A. Spisni, M. Cortsen, R. Muller, and P. Ring, V. in vivo field dependence of proton relaxation times in human brain, liver and skeletal muscle: A multicenter study, *in* "mri", volume 11, pp. 851-856, 1993.

[15] P. Bottomley, T. Foster, R. Argersinger, and L. Pfeifer, A review of tissue hydrogen NMR relaxation times and relaxation mechanisms from 1-100 MHz: Dependence on tissue type, NMR frequency, temperature, species, excision, and age, *Med. Phys.*, **11**, 425-448, (1984).

[16] G. Scott, S. Conolly, P. Morgan, and A. Macovski, Low cost controller for prepolarized MRI, *in* "Abstracts of the Society of Magnetic Resonance,4th Annual Meeting", p. 1386, New York, April 1996. Society of Magnetic Resonance.

[17] G. Scott, H. Xu, S. Conolly, and A. Macovski, Single conversion image reject receiver for low field MRI, *in* "Abstracts of the Int. Soc. Magnetic Resonance,5th Annual Meeting", p. 60, Vancouver, April 1997. Intl. Soc. of Magnetic Resonance.

[18] N. O. Fenzi and S. I. Long. Low noise preamplifier. U.S. Patent 5,488,382, 1996.

[19] G. Scott, S. Conolly, and A. Macovski, Low field preamp matching design for high Q receiver coils, *in* "Abstracts of the Society of Magnetic Resonance,4th Annual Meeting", p. 396, New York, April 1996. Society of Magnetic Resonance.

[20] M. Garrett, Thick cylindrical coil systems with field or gradient homogeneities of the 6th to 20th order, *J. Appl. Phys.*, **38**(6), 2563-2586, (1967).

[21] L. McKeehan, Combinations of circular currents for producing uniform magnetic fields., *R.S.I.*, **7**, 150—153, (1936).

[22] P. Morgan, S. Conolly, G. Scott, and A. Macovski, A readout magnet for prepolarized MRI, *Magn. Reson. Med.*, **36**, 527-536, (Oct. 1996).

[23] H. Xu, S. M. Conolly, G. Scott, and A. Macovski, Homogeneous magnet design using linear programming, *IEEE Transactions on Magnetics*, **36**(2), 476-483, (2000).

[24] D. B. Montgomery, "Solenoid Magnet Design". Krieger, Huntington, AL, 1980.

[25] S. M. Conolly, H. Xu, G. Scott, and A. Macovski, Edge cooling for low-field homogeneous magnets, *in* "Proceedings of the ISMRM", p. 1377, April 2000.

[26] N. Matter, S. Conolly, A. Macovski, and G. Scott, A fast recovery pulsed readout power supply for prepolarized MRI, *in* "Abstracts of the Int. Soc. Magnetic Resonance, 9th Annual Meeting", p. 1152, Glasgow, April 2001. Intl. Soc. of Magnetic Resonance.

[27] D. K. T. Claasen-Vujcic, H. Konijnenburg, J. Creyghton, J. Trommel, and A. Mehlkopf, Magnet system for very low field imaging, *in* "Abstracts of the Soc. Magnetic Resonance,3rd Annual Meeting", p. 933, Nice, Aug. 1995. Soc. of Magnetic Resonance.

[28] G. Scott, S. Conolly, and A. Macovski, Electromagnetic criteria for prepolarization coils, *in* "Abstracts of the Int. Soc. Magnetic Resonance, 8th Annual Meeting", p. 1373, Denver, April 2000. Intl. Soc. of Magnetic Resonance.

[29] S. Conolly, N. I. Matter, G. Scott, and A. Macovski, A high-power pulsing circuit for prepolarized MRI, *in* "Proceedings of the ISMRM", p. 473, April 1999.

[30] R. Turner, A target field approach to optimal coil design, *J. Phys. E: Scientific Instruments*, **19**, 147–151, (1986).

[31] R. Turner, Minimum inductance coils, *J. Phys. E: Scientific Instruments*, **21**, 948–952, (1988).

[32] R. Turner, Gradient coil design: a review of methods, *Magn. Reson. Imaging*, **11**, 903–20, (1993).

[33] E. Wong, A. Jesmanowicz, and J. Hyde, Coil optimization for MRI by conjugate gradient descent, *Magnetic Resonance in Medicine*, **21**, 39–48, (1991).

[34] E. Andrew and E. Szczesniak, Low inductance transverse gradient system of restricted length, *Magnetic Resonance Imaging*, **13**, 607–613, (1995).

[35] S. Crozier and D. Doddrell, Gradient-coil design by simulated annealing, *Journal of Magnetic Resonance*, **103**, 354, (1993).

[36] S. Crozier, L. Forbes, and D. Doddrell, The design of transverse gradient coils of restricted length by simulated annealing, *Journal of Magnetic Resonance A*, **107**, 126, (1994).

[37] S. Crozier and D. Doddrell, A design methodology for short whole body shielded gradient coils for MRI, *Magnetic Resonance Imaging*, **13**, 615, (1995).

9 Key Research Accomplishments

Our key research accomplishments in this grant were:

1. First *in vivo* Prepolarized MRI human images of the wrist. This breakthrough was presented at two oral presentations at the 2001 ISMRM. We demonstrated the first ever *in vivo* scans on a low-cost homebuilt prepolarized MRI scanner. The only previous attempt (by Toshiba researcher Joe Carlson) was on a commercial Toshiba scanner.

2. Greig Scott and graduate student Nathaniel Matter designed and constructed an ultra-stable switched current supply for controlling the readout magnet. This ultra-precise regulator stabilizes the readout current to better than a 50 parts per million while enabling significantly reduced heating of the readout magnet (due to the reduced duty cycle). The total hardware costs was less than $1,500. This was presented at the 2001 ISMRM.

3. We constructed and shimmed a new equiradius 3 MHz readout magnet with a 30-cm free bore. This magnet has a free bore more than double our hand imaging magnet, and water cooling so that it can operate at 3 times the field strength, or nine times the power. To accommodate these upgrades, we significantly simplified the overall mechanical design by using resistive shims instead of plate-mounted coils. The magnet cost ($6,720), which is only 40% of the cost of our hand-sized readout magnet ($17,000). We were able to shim this magnet to better than 50 ppm on axis. We had two abstracts on this magnet accepted to the 2000 ISMRM.

4. We have modified the linear programming algorithm developed in Year 1 to design shim coils. We are now constructing shim coils to improve the off-axis homogeneity of the 31 cm readout magnet. This was presented at the 2001 ISMRM.

5. Luchin Fay Wong developed our first dual transmit-receive RF coil, which was tested for the hand images shown in the grant. Total hardware cost was less than $200.

6. Our first experimental demonstration of human body noise dominance at under 5 MHz. This is a key technical verfication of the prepolarized MRI concept. Since we have experimentally shown that it is possible to create a pulsed readout field above 5 MHz, we can guarantee no loss of SNR relative to a conventional MRI scanner. Blaine Chronik gave a paper on this at the 2001 NMR Sensitivity Workshop at Berkeley.

7. First experimental contrast studies, including 1 mm resolution images of bacon, verifying that conventional T1 contrast is obtainable with PMRI. Also measured our first experimental T1 dispersion plots of chicken muscle and canola oil. These were all presented in oral presentations at the 2001 ISMRM at Glasgow.

8. We obtained our first phantom carefully demonstrating the linear dependence of signal with polarizing field strength. In fact we were able to increase the SNR by a factor of 24 with a polarizing field of 0.55 T. This was presented at the 2001 ISMRM.

9. We found that third-order damping of the readout magnet could greatly reduce transient ringing in the readout field. Without the new damping circuit, the readout magnet would ring for hundreds of milliseconds, rendering our PMRI experiment useless. The readout field is now stable within a few milliseconds of

the polarizing magnet rampdown. This new circuit enables PMRI to work.

10 Reportable Outcomes

1. "Homogeneous Magnet Design Using Linear Programming," Hao Xu, Steven Conolly, Greig Scott, Albert Macovski, *IEEE Transactions on Magnetics*, Vol. 36, No. 2, March 2000.

2. S. Mani, G. Luk Pat, S. Conolly, M. Moseley, D. Nishimura, and A. Macovski, "Multiple Inversion Recovery Perfusion," *Accepted by Magn. Reson. Med.*, 2000.

3. "Edge Cooling for Low-Field Homogeneous Magnets," Steven M. Conolly, Hao Xu, Greig C. Scott, Albert Macovski, *Proceedings of the ISMRM*, 2000.

4. "Split Resistive Shimming of Low-Field Homogeneous Magnets," Steven M. Conolly, Hao Xu, Greig C. Scott, Albert Macovski, *Proceedings of the ISMRM*, 2000.

5. "Electromagnetic Criteria for Prepolarization Coils," Greig C. Scott, Steven M. Conolly, Albert Macovski, *Proceedings of the ISMRM*, 2000.

6. "3D Echo Planar DEFT Imaging of Knee Cartilage," B.A. Hargreaves, J.M. Pauly, G.E. Gold, J. Tsai, P.K. Lang, S.M. Conolly, D.G. Nishimura, *Proceedings of the ISMRM*, 2000.

7. "Concomitant Gradient Effects in Spectral Spatial Pulses," Chi Ming Tsai, Craig Meyer, Steven M. Conolly, Dwight Nishimura, *Proceedings of the ISMRM*, 2000.

8. "A 31 cm Bore Readout Magnet for Prepolarized MRI" Hao Xu, Steven Conolly, Greig Scott, Albert Macovski, *Proceedings of the 41st ENC, Monterey CA*, poster 180, April 2000.

9. "Prepolarized Magnetic Resonance Imaging," S.M. Conolly, Invited Presentation of the ISMRM Workshop on MRI Hardware in Cleveland, February 24, 2001.

10. "Prepolarized Magnetic Resonance Imaging," S.M. Conolly Invited talk at the California Institute of Technology Biomedical Engineering 0.1 Seminar Series, March 16, 2001.

11. "A Prepolarized MRI Scanner," G. Scott, B. Chronik, N. Matter, H. Xu, P.N. Morgan, L. Wong, A. Macovski, S. Conolly, Proceedings of Int. Soc. Magnetic Resonance, 9th Annual Meeting, page 610, Glasgow, April, 2001.

12. Oscillating Dual-Equilibrium Steady State Angiography (ODESSA), W. Overall, S. Vasanawalla, S. Conolly, D. Nishimura and B. Hu, Proceedings of Int. Soc. Magnetic Resonance, 9th Annual Meeting, page 298, Glasgow, April, 2001.

13. A Universal Scaling Law for Optimizing Short Magnets, Gradient Coils, B. Zhang, C. Gazdzinski, B. Chronik, H. Xu, S. Conolly, B. Rutt, Abstracts of the Int. Soc. Magnetic Resonance, 9th Annual Meeting, page 614, Intl. Soc. of Magnetic Resonance, Glasgow, April, 2001.

14. "Signal and Contrast in Prepolarized MIR: First Data," S. Conolly, B. Chronik, N. Matter, P. Morgan, H. Xu, S. Ungersma, A. Macovski and G. Scott, Abstracts of the Int. Soc. Magnetic Resonance, 9th Annual Meeting, page 683, Intl. Soc. of Magnetic Resonance, Glasgow, April, 2001.

15. "Linear Programming Based Shim Design for Prepolarized MRI," S. Ungersma, A. Macovski, G. Scott and S. Conolly, Abstracts of the Int. Soc. Magnetic Resonance, 9th Annual Meeting, 1156, Intl.

Soc. of Magnetic Resonance, Glasgow, April, 2001.

16. "A Fast Recovery Pulsed Readout Power Supply for Prepolarized MRI," N. Matter, S. Conolly, A. Macovski, G. Scott, Abstracts of the Int. Soc. Magnetic Resonance, 9th Annual Meeting, page 1152, Intl. Soc. of Magnetic Resonance, Glasgow, April, 2001.

17. "Readout Frequency Requirements for Dedicated Prepolarized and Hyperpolarized-Gas MR Systems," B. Chronik, R. Venook, A. Macovski S. Conolly and G. Scott, Workshop on Limits of Detection in Nuclear Magnetic Resonance, 37, Intl. Soc. of Magnetic Resonance, Berkeley, June 2001.

18. Patent Issuance: Steven Conolly, "Minimum-Cost Polarizing Solenoids", pending, filed April 21, 1998. U.S. Patent 6,075,365 granted June 13, 2000. This patent covers a method for constructing a minimum cost polarizing coil for Prepolarized MRI. No effort made yet to commercialize.

19. Patent Issuance: Hao Xu, Steven Conolly, "Method for Designing Electromagnets having Arbitrary Geometrical Constraints," filing date 5/21/99. U.S. Patent 6,067,001, issued May 23, 2000. This patent application describes a general algorithm for designing electromagnets with arbitrary former constraints. We have found this to be very useful for low-cost gradient design, but there has been no effort yet to commercialize.

20. Patent Issuance: Hao Xu, Steven Conolly, Bob Hu "Short Bore-Length Asymmetric Electromagnets for MRI," field 5/21/99. U.S. Patent 6,064,290. This is a patent for a particular magnet with better patient and physician access. No effort yet to commercialize.

21. This biomedical engineering project has provided undergraduate research opportunities for many undergraduate students at Stanford including Ross Venook, Dave Pai, Alex Tung, Jack Wang, Serena Wong, Luchin Fay Wong, Karen Tisdale, Jaime Wong, Mike Ross and Lexyne McNealy. Lexyne is a visting student from Spelman College. The first six students were studying under a Stanford research award called the REU program.

22. Stanford Report wrote an article describing our research www.stanford.edu/group/mrsrl/intro.html.

23. Our research project has been profiled in *wired.com*, *Popular Science*, *Biophotonics International* (May 2001), and *The Silicon Valley Business Journal* (April 13, 2001), as well as several Radiology newsmagazines.

11 Personnel Receiving Pay

1. Albert Macovski, PhD
2. Steven Conolly, PhD
3. Greig Scott, PhD
4. Blaine Chronik, PhD
5. Hao Xu

12 Graduate Degrees resulting from the Support

Although none of the following students was completely supported on this grant but they did participate in the research.

1. Hao Xu has nearly completed his Doctoral dissertation in Electrical Engineering. He focused on tailoring the magnet geometry to the patient's anatomy.
2. Nathaniel Matter received his MSEE in 2000.
3. Ross Venook received his MSEE in 2001.
4. Sharon Ungersma received her Masters in Applied Physics in 2000.

13 Bibliography of Publications from Support

1. "Resistive Homogeneous MRI Magnet Design by Matrix Subset Selection," Patrick N. Morgan, Steven M. Conolly, Albert Macovski, *Magn Reson Med.*, 41(6):1221-9, June 1999.
2. "MR Imaging of Articular Cartilage using Driven Equilibrium," Brian A. Hargreaves, Garry E. Gold, Phillip K. Lang, Steven M. Conolly, John M. Pauly, G. Bergman, J. Vandevenne, and Dwight G. Nishimura, *Magn Reson Med.*, 42(4):695-703, Oct. 1999.
3. "Homogeneous Magnet Design Using Linear Programming," Hao Xu, Steven Conolly, Greig Scott, Albert Macovski, *IEEE Transactions on Magnetics*, Vol. 36, No. 2, March 2000.
4. "Fundamental Scaling Relations for Homogeneous Magnets," H. Xu, G.C. Scott, A. Macovski, and S.M. Conolly *Submitted to Magn. Reson. Medicine*, 2001.
5. "Prepolarized Magnetic Resonance Imaging," Eighth Annual Little Rock Workshop on Advances in NMR Engineering, June 3-4, 1999.
6. "Prepolarized Magnetic Resonance Imaging," S.M. Conolly, Invited Presentation of the ISMRM Workshop on MRI Hardware in Cleveland, February 24, 2001.
7. "Prepolarized Magnetic Resonance Imaging," S.M. Conolly Invited talk at the California Institute of Technology Biomedical Engineering 0.1 Seminar Series, March 16, 2001.
8. "Minimum Power Homogeneous Magnet Design for Prepolarized MRI," H. Xu, S.M. Conolly, G. Scott and A. Macovski, *Proceedings of the ISMRM*, p. 2006, 1998.

9. "Polyphase Techniques for Low Cost MRI Receivers," G. Scott, S. Conolly and A. Macovski, *Proceedings of the ISMRM*, p. 2020, 1998.

10. "Minimum-Cost Solenoid Design for Prepolarized MRI," S.M. Conolly, G.C. Scott and A. Macovski. *Proceedings of the ISMRM*, p. 255, 1998.

11. "Fundamental Scaling Relations for Homogeneous Magnets," H. Xu, S.M. Conolly, G.C. Scott and A. Macovski. *Proceedings of the ISMRM*, 1999.

12. "Gradient Design with Arbitrary Geometrical Constraints by Linear Programming," H. Xu, S.M. Conolly, G.C. Scott and A. Macovski. *Proceedings of the ISMRM*, 1999.

13. "A High-Power Pulsing Circuit for Prepolarized MRI," S.M. Conolly, N.I. Matter, G.C. Scott and A. Macovski. *Proceedings of the ISMRM*, 1999.

14. "Electromagnet Current Regulation with Thyristor Supplies," G.C. Scott, H. Xu, S.M. Conolly, A. Macovski. *Proceedings of the ISMRM*, 1999.

15. "Design of Dedicated Shim Fields," E. Adalsteinsson, S.M. Conolly, H. Xu, A. Macovski. *Proceedings of the ISMRM*, 1999.

16. "Edge Cooling for Low-Field Homogeneous Magnets," Steven M. Conolly, Hao Xu, Greig C. Scott, Albert Macovski, *Proceedings of the ISMRM*, 2000.

17. "Split Resistive Shimming of Low-Field Homogeneous Magnets," Steven M. Conolly, Hao Xu, Greig C. Scott, Albert Macovski, *Proceedings of the ISMRM*, 2000.

18. "Electromagnetic Criteria for Prepolarization Coils," Greig C. Scott, Steven M. Conolly, Albert Macovski, *Proceedings of the ISMRM*, 2000.

19. "3D Echo Planar DEFT Imaging of Knee Cartilage," B.A. Hargreaves, J.M. Pauly, G.E. Gold, J. Tsai, P.K. Lang, S.M. Conolly, D.G. Nishimura, *Proceedings of the ISMRM*, 2000.

20. "Concomitant Gradient Effects in Spectral Spatial Pulses," Chi Ming Tsai, Craig Meyer, Steven M. Conolly, Dwight Nishimura, *Proceedings of the ISMRM*, 2000.

21. "A 31 cm Bore Readout Magnet for Prepolarized MRI" Hao Xu, Steven Conolly, Greig Scott, Albert Macovski, *Proceedings of the 41st ENC, Monterey CA*, poster 180, April 2000.

22. "A Prepolarized MRI Scanner," G. Scott, B. Chronik, N. Matter, H. Xu, P.N. Morgan, L. Wong, A. Macovski, S. Conolly, Proceedings of Int. Soc. Magnetic Resonance, 9th Annual Meeting, page 610, Glasgow, April, 2001,

23. Oscillating Dual-Equilibrium Steady State Angiography (ODESSA), W. Overall, S. Vasanawalla, S. Conolly, D. Nishimura and B. Hu, Proceedings of Int. Soc. Magnetic Resonance, 9th Annual Meeting, page 298, Glasgow, April, 2001.

24. A Universal Scaling Law for Optimizing Short Magnets, Gradient Coils, B. Zhang, C. Gazdzinski, B. Chronik, H. Xu, S. Conolly, B. Rutt, Abstracts of the Int. Soc. Magnetic Resonance, 9th Annual Meeting, page 614, Intl. Soc. of Magnetic Resonance, Glasgow, April, 2001.

25. "Signal and Contrast in Prepolarized MIR: First Data," S. Conolly, B. Chronik, N. Matter, P. Morgan, H. Xu, S. Ungersma, A. Macovski and G. Scott, Abstracts of the Int. Soc. Magnetic Resonance, 9th Annual

Meeting, page 683, Intl. Soc. of Magnetic Resonance, Glasgow, April, 2001.

26. "Linear Programming Based Shim Design for Prepolarized MRI," S. Ungersma, A. Macovski, G. Scott and S. Conolly, Abstracts of the Int. Soc. Magnetic Resonance, 9th Annual Meeting, 1156, Intl. Soc. of Magnetic Resonance, Glasgow, April, 2001.

27. "A Fast Recovery Pulsed Readout Power Supply for Prepolarized MRI," N. Matter, S. Conolly, A. Macovski, G. Scott, Abstracts of the Int. Soc. Magnetic Resonance, 9th Annual Meeting, page 1152, Intl. Soc. of Magnetic Resonance, Glasgow, April, 2001.

28. "Readout Frequency Requirements for Dedicated Prepolarized and Hyperpolarized-Gas MR Systems," B. Chronik, R. Venook, A. Macovski S. Conolly and G. Scott, Workshop on Limits of Detection in Nuclear Magnetic Resonance, 37, Intl. Soc. of Magnetic Resonance, Berkeley, June 2001.